Time-dependent Schrödinger equation for molecular core-hole dynamics

A. Picón*
Argonne National Laboratory, Argonne, Illinois 60439, USA
(Received 22 November 2016; published 1 February 2017)

X-ray spectroscopy is an important tool for the investigation of matter. X rays primarily interact with inner-shell electrons, creating core (inner-shell) holes that will decay on the time scale of attoseconds to a few femtoseconds through electron relaxations involving the emission of a photon or an electron. The advent of femtosecond x-ray pulses expands x-ray spectroscopy to the time domain and will eventually allow the control of core-hole population on time scales comparable to core-vacancy lifetimes. For both cases, a theoretical approach that accounts for the x-ray interaction while the electron relaxations occur is required. Here we describe a time-dependent framework, based on solving the time-dependent Schrödinger equation, that is suitable for describing the induced electron and nuclear dynamics.

DOI: 10.1103/PhysRevA.95.023401

I. INTRODUCTION

Over nearly a century, x rays have evolved into an important tool for spectroscopic applications primarily due to their element specificity [1]. X-ray absorption, emission, and Auger as well as photoelectron spectroscopy have been used to investigate systems ranging from atoms and molecules in the gas phase [2] to surfaces, interfaces, and solids [3].

Over the past decades optical spectroscopy has rapidly progressed towards time-resolved approaches. The advent of femtosecond laser spectroscopy opened the possibility to observe very fast nuclear dynamics and have access to resolve even the vibrational motion of some molecular systems in real time. The wide active area of research that resorts to those time-resolved studies is nowadays known as femtochemistry [4]. In the field of femtochemistry, the common experimental setup is the use of two femtosecond optical lasers; the first one, the pump, excites the molecule, while the second one, the probe, probes the induced molecular dynamics. Femtosecond laser spectroscopy has provided real-time studies of dynamics in chemical reactions, materials, and biological systems.

The field of time-resolved x-ray spectroscopy has developed in recent years [5,6], and ultraintense femtosecond pulses from free-electron lasers have opened the door for ultrafast investigations on time scales similar to core-vacancy decay [7–10]. New approaches for pump-probe techniques involving inner-shell electrons using either optical pump schemes at high-harmonic sources [11–16] or xuv [17,18] and x-ray pump schemes at free-electron lasers [19–22] are pursued.

From the fundamental point of view, the x-ray interaction of such short pulses with matter yields interesting questions to explore, as the time scale of the x-ray probing is comparable to the electron relaxation processes triggered by the absorption of the same x-ray pulse. When an x-ray photon is absorbed by a molecule, a core electron is promoted into a highly excited state, leaving behind a core-hole state. Those states are quite unstable and decay rapidly between hundreds of attoseconds and a few femtoseconds. Hence, it is possible to tailor the dynamics of the core-hole states before their decay, a unique feature of these ultrashort x-ray pulses. The understanding of this interaction is crucial for the development of unprecedented nonlinear spectroscopy methods with few-femtosecond and attosecond time resolution [23].

The theoretical models for x-ray spectroscopy are still mostly tailored towards the static case [2], but in light of the rapidly developing time-resolved x-ray experiments new time-dependent theoretical approaches are needed. In this paper I describe a time-dependent approach that is based on a time-dependent Schrödinger equation formalism that includes core-level states, which are relevant to x-ray spectroscopy. Similar time-dependent approaches have been developed in the past in the context of vibrational interference effects on autoionizing electron spectra [24]. The approach introduced here can describe both resonant and nonresonant x-ray excitations. The formalism is benchmarked against x-ray absorption and Auger emission data of diatomic molecules and it shows excellent agreement with experimental spectra. With the time-dependent Schrödinger approach we have a tool at hand to describe time-resolved experiments in the x-ray domain that can easily be expanded to larger systems.

II. THE THEORETICAL MODEL

The theoretical approach is based on solving the time-dependent Schrödinger equation (TDSE) restricted to those electronic states that are involved in the main dynamics. In a molecule, the Hamiltonian may be written in two terms, the electronic and nuclear Hamiltonian,

$$\hat{H}_0 = \hat{H}_e + \hat{H}_n, \tag{1}$$

where

$$\hat{H}_e = \sum_j \hat{K}_j + \sum_{ij} \hat{V}_{ij}^{(pe)} + \sum_{j>j'} \hat{V}_{jj'}^{(ee)}, \tag{2}$$

$$\hat{H}_n = \sum_i \hat{K}_i + \sum_{i>i'} \hat{V}_{ii'}^{(pp)}. \tag{3}$$

*antonio.picon.alvarez@gmail.com; present address: Grupo de Investigación en Aplicaciones del Láser y Fotónica, Departamento de Física Aplicada, University of Salamanca, E-37008, Salamanca, Spain.

The wave function of the system depends on both the electronic and nuclear coordinates $\Psi = \Psi(\mathbf{X},\mathbf{R})$, where $\mathbf{X} = \{\mathbf{x_1},\mathbf{x_2},\ldots,\mathbf{x_j},\ldots,\mathbf{x_N}\}$ and $\mathbf{R} = \{\mathbf{R_1},\mathbf{R_2},\ldots,\mathbf{R_i},\ldots,\mathbf{R_M}\}$. The wave function can be expanded as $\Psi = \sum_a b_a^{(e)}(\mathbf{R})\Phi_a^{(e)}(\mathbf{X},\mathbf{R})$, with $\Phi_a^{(e)}$ being an eigenstate of the electronic Hamiltonian for a specific nuclear coordinate $\mathbf{R}$, that is,

$$\hat{H}_e\Phi_a^{(e)}(\mathbf{X},\mathbf{R}) = E_a^{(e)}(\mathbf{R})\Phi_a^{(e)}(\mathbf{X},\mathbf{R})\,. \tag{4}$$

Calculating the Coulomb electron repulsion of all electrons is an impossible task for molecules having more than two electrons. It is the aim of quantum chemistry codes to perform calculations approximating the Coulomb repulsion and obtaining a solution close to considering all electron correlations. In general, we can always assume that the electronic Hamiltonian of the system is composed by two terms,

$$\hat{H}_e = \hat{H}_{\text{eff}} + \hat{V}_r, \tag{5}$$

where $\hat{H}_{\text{eff}}$ is the effective Hamiltonian that approximates the electron correlations and $\hat{V}_r$ is the residual term. The better our approximation to the electron correlations is, the smaller the contribution of the residual potential is. Within the Hilbert space given by the effective Hamiltonian, the wave function can be expanded as $\Psi = \sum_a b_a(\mathbf{R})\Phi_a(\mathbf{X},\mathbf{R})$, with Φ_a now being an eigenstate of the effective Hamiltonian,

$$\hat{H}_{\text{eff}}\Phi_a(\mathbf{X},\mathbf{R}) = E_a(\mathbf{R})\Phi_a(\mathbf{X},\mathbf{R}). \tag{6}$$

The total Hamiltonian of the molecule is expanded, by using ansatz (1), as

$$\hat{H}_0\Psi = \sum_a \Phi_a(\mathbf{X},\mathbf{R})[\hat{H}_n + E_a(\mathbf{R}) + \hat{V}_r(\mathbf{R})]b_a(\mathbf{R}) + \sum_a b_a(\mathbf{R})\left[\sum_i \hat{K}_i\Phi_a(\mathbf{X},\mathbf{R})\right]. \tag{7}$$

In the Born-Oppenheimer (BO) approximation, the change in the nuclear wave packet is considered to be much slower in time than the electronic wave packet, and the second term in Eq. (7) is neglected during the time evolution. If we consider the coupling with an electromagnetic wave field $V_I(t)$, the total Hamiltonian $\hat{H}(t) = \hat{H}_0 + V_I(t)$ is time dependent, and then our wave function will have an explicit dependence on time as $\Psi(t) = \sum_a b_a(\mathbf{R},t)\Phi_a(\mathbf{X},\mathbf{R})$. Assuming that the external field mainly couples with the electrons, the total Hamiltonian is, within the dipole approximation,

$$\hat{H}(t)\Psi(t) = \sum_a \Phi_a(\mathbf{X},\mathbf{R})[\hat{H}_n + E_a(\mathbf{R}) + \hat{V}_r(\mathbf{R}) + V_I(t)]b_a(\mathbf{R},t) + \sum_a b_a(\mathbf{R},t)\left[\sum_i \hat{K}_i\Phi_a(\mathbf{X},\mathbf{R})\right]. \tag{8}$$

The time evolution of the quantum system will be described by the time-dependent Schrödinger equation $i\partial\Psi(t)/\partial t = \hat{H}(t)\Psi(t)$; using Eq. (8), this is

$$i\sum_a \dot{b}_a(\mathbf{R},t)\Phi_a(\mathbf{X},\mathbf{R}) = \sum_a \Phi_a(\mathbf{X},\mathbf{R})[\hat{H}_n + V_I(t) + E_a(\mathbf{R}) + \hat{V}_r(\mathbf{R})]b_a(\mathbf{R},t) + \sum_a b_a(\mathbf{R},t)\left[\sum_i \hat{K}_i\Phi_a(\mathbf{X},\mathbf{R})\right]. \tag{9}$$

We can interpret the written time-dependent Schrödinger equation as nuclear wave packets propagating along different potential-energy surfaces (PESs), and those nuclear wave packets can jump to different electronic PESs via the light interaction and nonadiabatic couplings, and also via the residual potential V_r couplings. Note that the nuclear wave-packet amplitudes $b_a(\mathbf{R},t)$ are in the space representation, instead of using the conventional expansion in vibrational states. This has a numerical advantage in solving the TDSE for ultrashort pulses. In the common ultrafast experiments, the molecule is in the ground state or some low-lying excited state. The ultrashort pulse excites the molecule into several states, but due to the localized action of the light-interaction coupling, the excited superposition is well localized in space. If the time scale of the interaction is on the order of hundreds of femtoseconds, we can contain the entire wave function in a small spatial grid. With this spatial representation we do not need to calculate explicitly vibrational or dissociative states.

Solving the complete TDSE is quite demanding, and for numerical purposes, it is a better strategy to limit the electronic states to those that are important during the time evolution of the system. Similar models have been used before (see, for example, Refs. [22,24,25]). In the following, we discuss in detail two particular cases of the time-dependent Schrödinger equation for inner-shell dynamics (TDSE-IS), the nonresonant and resonant core excitations with Auger decay. However, this approach is quite general, and it can be extended to more complex systems by considering more electronic states.

A. Nonresonant core excitation

In this section we consider the physical scenario that a core electron is ionized, leaving behind a core-hole state. We will assume that the core-hole state mainly decays by Auger processes (this is the case for light atomic elements). We restrict the ansatz of the system to

$$\psi(t) = b_0(\mathbf{R},t)\Phi_0(\mathbf{X},\mathbf{R}) + \sum_\varepsilon\sum_i b_{\varepsilon;i}(\mathbf{R},t)\Phi_{\varepsilon;i}(\mathbf{X},\mathbf{R}) + \sum_{\varepsilon\varepsilon_a}\sum_{ij} b_{\varepsilon\varepsilon_a;ij}(\mathbf{R},t)\Phi_{\varepsilon\varepsilon_a;ij}(\mathbf{X},\mathbf{R}), \tag{10}$$

where b_0 stands for the amplitude of the ground state, $b_{\varepsilon;i}$ stands for the core-hole states after x-ray photoionization, and $b_{\varepsilon\varepsilon_a;ij}$ stands for the final states after Auger decay. Using the ansatz (10) in Eq. (9) and projecting onto a specific electronic state and integrating over the electron coordinates, we obtain

a system of equations of motion (EOMs) for the amplitudes

$$i\,\dot{b}_0(\mathbf{R},t) = [\hat{H}_n + E_0(\mathbf{R})]\,b_0(\mathbf{R},t) + \sum_{\varepsilon}\sum_{i}\langle 0|V_I(t)|\varepsilon;i\rangle\, b_{\varepsilon;i}(\mathbf{R},t), \quad (11)$$

$$i\,\dot{b}_{\varepsilon;i}(\mathbf{R},t) = [\hat{H}_n + E_{\varepsilon;i}(\mathbf{R})]b_{\varepsilon;i}(\mathbf{R},t) + \langle\varepsilon;i|V_I(t)|0\rangle\, b_0(\mathbf{R},t) + \sum_{\varepsilon'\neq\varepsilon}\sum_{i'\neq i}\langle\varepsilon;i|V_r|\varepsilon';i'\rangle\, b_{\varepsilon';i'}(\mathbf{R},t) + \sum_{\varepsilon'\varepsilon'_a}\sum_{i'j'}\langle\varepsilon;i|V_r|\varepsilon'\varepsilon'_a;i'j'\rangle\, b_{\varepsilon'\varepsilon'_a;i'j'}(\mathbf{R},t), \quad (12)$$

$$i\,\dot{b}_{\varepsilon\varepsilon_a;ij}(\mathbf{R},t) = \left[\hat{H}_n + E_{\varepsilon\varepsilon_a;ij}(\mathbf{R})\right] b_{\varepsilon\varepsilon_a;ij}(\mathbf{R},t) + \sum_{\varepsilon'}\sum_{i'}\langle\varepsilon\varepsilon_a;ij|V_r|\varepsilon';i'\rangle\, b_{\varepsilon';i'}(\mathbf{R},t) + \sum_{\varepsilon'\varepsilon'_a\neq\varepsilon\varepsilon_a}\sum_{i'j'\neq ij}\langle\varepsilon\varepsilon_a;ij|V_r|\varepsilon'\varepsilon'_a;i'j'\rangle \times b_{\varepsilon'\varepsilon'_a;i'j'}(\mathbf{R},t), \quad (13)$$

where

$$\langle a|V_I(t)|a'\rangle = \int d\mathbf{X}\;\; \Phi^*_a(\mathbf{X},\mathbf{R})\; V_I(t)\; \Phi_{a'}(\mathbf{X},\mathbf{R}),$$

$$\langle a|V_r|a'\rangle = \int d\mathbf{X}\;\; \Phi^*_a(\mathbf{X},\mathbf{R})\; V_r(\mathbf{R})\; \Phi_{a'}(\mathbf{X},\mathbf{R}).$$

The energies of the ground state, core-excited states, and final states are given by E_0, $E_{\varepsilon;i}$, and $E_{\varepsilon\varepsilon_a;ij}$, respectively. We have neglected the nonadiabatic coupling in Eq. (9); also, the terms

$$\langle\varepsilon;i|\hat{V}_r|0\rangle \approx 0, \quad \langle\varepsilon\varepsilon_a;ij|\hat{V}_r|0\rangle \approx 0$$

are not considered, as they are quite small compared to the other dominant terms that we discuss in the following.

In core-shell ionization, when the ionization may come from several degenerate states or states close in energy, for example, the ionization of $3d$ electrons in Xe or C $1s$ electrons in acetylene, the random-phase approximation (RPA) at the Hartree-Fock level or the multichannel Hartree-Fock theory provides a good theoretical description of the involved electron correlations (see, for example, Refs. [2,26–29]). The RPA has also been applied at the level of algebraic-diagrammatic construction (ADC) [30]. The RPA can also be applied in the calculations of Auger decay transitions [31]. In these approaches, the couplings between different channels in the final state are considered. In this work, we consider those electron-correlation couplings to be zero, that is,

$$\langle\varepsilon;i|V_r|\varepsilon';i'\rangle \approx 0, \quad \langle\varepsilon\varepsilon_a;ij|V_r|\varepsilon'\varepsilon'_a;i'j'\rangle \approx 0.$$

The system of equations (11)–(13) can be further decoupled by using the adiabatic approximation, also known as local approximation [32,33]. The adiabatic approximation can be applied to the ionization step, which is known in the quantum optics community as Markov approximation [34,35], and to the Auger decay step. Within these approximations (see more details in the Appendix), the EOMs can be reduced with the derivation of decay rates Γ that accounts for the ionization of the ground state and the Auger decay of the core-hole state and Stark shifts R that account for the dephasing introduced by the continuum part that has been decoupled:

$$\begin{aligned}
i\,\dot{b}_0(\mathbf{R},t) &= [\hat{H}_n + E_0(\mathbf{R})]\,b_0(\mathbf{R},t) - i\left[\frac{\Gamma_I(\mathbf{R},t)}{2} + i\,R_I(\mathbf{R},t)\right]b_0(\mathbf{R},t) \\
&\quad - \sum_{\varepsilon}\sum_{i}\langle 0|V_I|\varepsilon;i\rangle\int_{t_0}^{t}dt'\sum_{\varepsilon'\neq\varepsilon}\sum_{i'\neq i}\left[\frac{\Gamma_{\varepsilon i,\varepsilon' i'}(\mathbf{R})}{2} + i\,R_{\varepsilon i,\varepsilon' i'}(\mathbf{R})\right]b_{\varepsilon';i'}(\mathbf{R},t')\; e^{-i[E_{\varepsilon;i}(\mathbf{R})+R_{\varepsilon i,\varepsilon i}(\mathbf{R})-i\Gamma_{\varepsilon i,\varepsilon i}(\mathbf{R})/2](t-t')}, \\
i\,\dot{b}_{\varepsilon;i}(\mathbf{R},t) &= [\hat{H}_n + E_{\varepsilon;i}(\mathbf{R})]b_{\varepsilon;i}(\mathbf{R},t) + \langle\varepsilon;i|V_I(t)|0\rangle\, b_0(\mathbf{R},t) - i\sum_{\varepsilon'}\sum_{i'}\left[\frac{\Gamma_{\varepsilon i,\varepsilon' i'}(\mathbf{R})}{2} + i\,R_{\varepsilon i,\varepsilon' i'}(\mathbf{R})\right]b_{\varepsilon';i'}(\mathbf{R},t), \\
i\,\dot{b}_{\varepsilon\varepsilon_a;ij}(\mathbf{R},t) &= \left[\hat{H}_n + E_{\varepsilon\varepsilon_a;ij}(\mathbf{R})\right] b_{\varepsilon\varepsilon_a;ij}(\mathbf{R},t) + \sum_{\varepsilon'}\sum_{i'}\langle\varepsilon\varepsilon_a;ij|V_r|\varepsilon';i'\rangle\, b_{\varepsilon';i'}(\mathbf{R},t),
\end{aligned} \quad (14)$$

where

$$\frac{\Gamma_{\varepsilon i,\varepsilon' i'}(\mathbf{R})}{2} = \pi\sum_{\varepsilon''\varepsilon''_a}\sum_{i''j''}\langle\varepsilon;i|V_r|\varepsilon''\varepsilon''_a;i''j''\rangle\,\langle\varepsilon''\varepsilon''_a;i''j''|V_r|\varepsilon';i'\rangle\;\;\delta\left(E_{\varepsilon''\varepsilon''_a;i''j''} - E_{\varepsilon';i'}\right),$$

$$R_{\varepsilon i,\varepsilon' i'}(\mathbf{R}) = -i\sum_{\varepsilon''\varepsilon''_a}\sum_{i''j''}\langle\varepsilon;i|V_r|\varepsilon''\varepsilon''_a;i''j''\rangle\,\langle\varepsilon''\varepsilon''_a;i''j''|V_r|\varepsilon';i'\rangle\;\;P\left[\frac{1}{E_{\varepsilon''\varepsilon''_a;i''j''} - E_{\varepsilon';i'}}\right],$$

$$\frac{\Gamma_I(\mathbf{R},t)}{2} = \frac{\Omega^2(t)}{4}\sum_{\varepsilon}\sum_{i}\langle 0|\tilde{V}_I|\varepsilon;i\rangle\langle\varepsilon;i|\tilde{V}_I|0\rangle\frac{\Gamma_{\varepsilon i,\varepsilon i}/2}{(E_{\varepsilon;i} + R_{\varepsilon i,\varepsilon i} - E_0 - \omega)^2 + (\Gamma_{\varepsilon i,\varepsilon i}/2)^2},$$

$$R_I(\mathbf{R},t) = -\frac{\Omega^2(t)}{4}\sum_{\varepsilon}\sum_{i}\langle 0|\tilde{V}_I|\varepsilon;i\rangle\langle\varepsilon;i|\tilde{V}_I|0\rangle\frac{E_{\varepsilon;i} + R_{\varepsilon i,\varepsilon i} - E_0 - \omega}{(E_{\varepsilon;i} + R_{\varepsilon i,\varepsilon i} - E_0 - \omega)^2 + (\Gamma_{\varepsilon i,\varepsilon i}/2)^2}.$$

The symbol P stands for the principal value. The Rabi frequency of the pulse is given by $\Omega(t)$, the frequency of the pulse is given by ω, and the dipole moments between the ground state and core-hole states is given by $\langle 0|\tilde{V}_I|\varepsilon;i\rangle$, where $\tilde{V}_I$ stands for the electric dipole moment, i.e., $-\sum_j q_j\,\mathbf{r}_j\cdot\mathbf{s}$, where $\mathbf{s}$ is the polarization direction. The ionization rate of the ground state is related to the term $\Gamma_I(t)$, which depends on the envelope (intensity) of the pulse. The Auger transitions are given by the couplings $\langle\varepsilon;i|V_r|\varepsilon''\varepsilon_a'';i''j''\rangle$. The decay of the core-excited state is related to the term $\Gamma_{\varepsilon i,\varepsilon i}$, which is the sum of all Auger transitions allowed in the system.

B. Resonant core excitation

In this section we consider the physical scenario in which a core electron is promoted into a bound highly excited state, leaving behind a core-hole state. After core resonant excitation, the system is still neutral (no loss of electrons). We will assume that the core-hole state mainly decays by Auger processes. Like in the nonresonant case, we limit the Hilbert space to the electronic states mainly involved in the dynamics. We consider the ansatz of the system to be

$$\psi(t) = b_0(\mathbf{R},t)\Phi_0(\mathbf{X},\mathbf{R}) + b_c(\mathbf{R},t)\Phi_c(\mathbf{X},\mathbf{R}) + \sum_{\varepsilon_a}\sum_{ij} b_{c\varepsilon_a;ij}(\mathbf{R},t)\Phi_{c\varepsilon_a;ij}(\mathbf{X},\mathbf{R}), \tag{15}$$

where b_0 is the amplitude of the ground state, b_c is the core-hole state after resonant excitation, and $b_{c\varepsilon_a;ij}$ are the final states after Auger decay. Using the ansatz (15) in Eq. (9), projecting onto a specific electronic state, and integrating over the electron coordinates, we obtain the EOMs for the resonant excitation:

$$\begin{aligned}
i\,\dot{b}_0(\mathbf{R},t) &= [\hat{H}_n + E_0(\mathbf{R})]\,b_0(\mathbf{R},t) + \langle 0|V_I(t)|c\rangle\,b_c(\mathbf{R},t),\\
i\,\dot{b}_c(\mathbf{R},t) &= [\hat{H}_n + E_c(\mathbf{R})]b_c(\mathbf{R},t) + \langle c|V_I(t)|0\rangle\,b_0(\mathbf{R},t)\\
&\quad + \sum_{\varepsilon_a'}\sum_{i'j'}\langle c|V_r|c\,\varepsilon_a';i'j'\rangle\,b_{c\varepsilon_a';i'j'}(\mathbf{R},t),\\
i\,\dot{b}_{c\varepsilon_a;ij}(\mathbf{R},t) &= \left[\hat{H}_n + E_{c\varepsilon_a;ij}(\mathbf{R})\right]b_{c\varepsilon_a;ij}(\mathbf{R},t)\\
&\quad + \langle c\,\varepsilon_a;ij|V_r|c\rangle\,b_c(\mathbf{R},t)\\
&\quad + \sum_{\varepsilon_a'\neq\varepsilon_a}\sum_{i'j'\neq ij}\langle c\,\varepsilon_a;ij|V_r|c\,\varepsilon_a';i'j'\rangle\\
&\quad \times b_{c\varepsilon_a';i'j'}(\mathbf{R},t).
\end{aligned} \tag{16}$$

We can decouple the EOMs by using the adiabatic approximation in the Auger step and further reduce the EOMs by using decay rates Γ and Stark shift R parameters. Within the adiabatic approximation, neglecting the RPA terms, we obtain

$$\begin{aligned}
i\,\dot{b}_0(\mathbf{R},t) &= [\hat{H}_n + E_0(\mathbf{R})]\,b_0(\mathbf{R},t) + \langle 0|V_I(t)|c\rangle\,b_c(\mathbf{R},t),\\
i\,\dot{b}_c(\mathbf{R},t) &= [\hat{H}_n + E_c(\mathbf{R})]b_c(\mathbf{R},t) + \langle c|V_I(t)|0\rangle\,b_0(\mathbf{R},t)\\
&\quad - i\left[\frac{\Gamma_c(\mathbf{R})}{2} + i\,R_c(\mathbf{R})\right]b_c(\mathbf{R},t),\\
i\,\dot{b}_{c\varepsilon_a;ij}(\mathbf{R},t) &= \left[\hat{H}_n + E_{c\varepsilon_a;ij}(\mathbf{R})\right]b_{c\varepsilon_a;ij}(\mathbf{R},t)\\
&\quad + \langle c\varepsilon_a;ij|V_r|c\rangle\,b_c(\mathbf{R},t),
\end{aligned} \tag{17}$$

where

$$\frac{\Gamma_c(\mathbf{R})}{2} = \pi\sum_{\varepsilon_a'}\sum_{i'j'}|\langle c\,\varepsilon_a';i'j'|V_r|c\rangle|^2\,\delta\left(E_{c\varepsilon_a';i'j'} - E_c\right),$$

$$R_c(\mathbf{R}) = -i\sum_{\varepsilon_a'}\sum_{i'j'}|\langle c\,\varepsilon_a';i'j'|V_r|c\rangle|^2\;P\left[\frac{1}{E_{c\varepsilon_a';i'j'} - E_c}\right].$$

III. NUMERICAL IMPLEMENTATION

In the introduced theoretical model, the time evolution of the system is governed by EOMs such as Eqs. (14) and (17). By calculating all the electronic properties at different nuclear geometries (energies, electric dipole transitions, and Auger dipole transitions), the numerical problem reduces to solving a system of coupled ordinary differential equations. For that purpose, we can use common numerical methods such as Runge-Kutta or Crank-Nicolson methods.

The electronic calculations can be calculated with standard quantum chemistry codes, in addition to those matrix elements involving continuum orbitals. Most common quantum chemistry codes are based on multicenter grids expanded with a localized basis set, most commonly the Gaussian basis. To calculate the energies of the ground state, core-hole states, and final state, we need first to choose a level of description for the electronic correlations, for example, Hartree-Fock (HF), configuration interaction (CI), coupled cluster (CC), and multireference CI (MRCI), which determines the Hamiltonian H_{eff} and the residual V_r. Often, for a better description of the system, we need to use a different level of electron correlations for different electronic states. For example, the core-hole state energies have a high degree of electron relaxation, and a second self-consistent field (SCF) calculation by imposing a hole in the corresponding core orbital results in much better accuracy [36–38]. If we consider electronic states with different H_{eff}, then we need to modify correspondingly the EOMs given by Eqs. (14) and (17) by including terms with overlapping factors, as the eigenstates would no longer be orthogonal.

Most quantum chemistry codes do not include the possibility to calculate continuum orbitals, which are needed for obtaining matrix elements such as electric dipole (ionization) and Auger transitions. There are several approaches to calculate continuum orbitals, such as Dyson orbital methods [39,40] or single-center expansions based on scattering theory [41–44]. Stieltjes imaging is often used in the literature to obtain observables such as photoionization cross sections [45,46] and Auger decay transitions [47]. However, this method does not allow us to obtain the continuum waves required for the TDSE-IS.

The initial state $b_0(\mathbf{R},t_0)$ has to be calculated prior to solving the TDSE-IS. Once we have the PES for the ground state, we can diagonalize the nuclear Hamiltonian, in the absence of any external field, to obtain the vibrational states of the ground state, or we can use an imaginary time-evolution method for this purpose.

IV. COMPARISON WITH EXPERIMENTAL DATA

By solving the TDSE-IS we can calculate the most relevant observables to be measured in experiments, even in static experiments, such as x-ray absorption and Auger spectra. In

the following section we explain in detail how to calculate those observables within this time-dependent framework and compare it to previously published experimental results.

A. X-ray absorption spectroscopy

X-ray absorption spectroscopy is a very common technique at synchrotrons. Nowadays, that technique has been highly refined, mainly due to the experimental advances in selecting and tuning the photon energy of the x-ray pulses with a narrow bandwidth. In an x-ray absorption spectrum we can distinguish two domains: the x-ray absorption near-edge structure (XANES) and the extended x-ray absorption fine structure (EXAFS), corresponding to low and high photon energies, respectively. XANES contains information about the resonant excitations and continuum excitations near resonances, providing information about the electronic configuration and local chemical environment with respect to the absorber. EXAFS is the high-energy domain where continuum photoelectrons are dominated by single-scattering events, providing information about the coordination number, type, and distance of ligating atoms with respect to the absorber. X-ray absorption spectroscopy is a powerful spectroscopic technique that is used in a wide range of applications ranging from photochemistry and solar energy conversion [48–51], interfacial electron transfer in photocatalysis, and biological enzymatic systems [52] to materials characterization.

We start discussing the case of static x-ray absorption spectroscopy. The time evolution of the system is given by the nuclear wave-packet amplitudes obtained by solving the TDSE-IS. At the end of the x-ray pulse interaction, the system keeps evolving (electron relaxations and nuclear propagation), but the population in the ground state will remain constant. The difference in population of what we have at the beginning and what we have after the x-ray pulse in the ground state will be related to the absorption signal for a specific photon energy. If we perform the TDSE-IS using x-ray pulses with different photon energies, we can then obtain the x-ray absorption spectrum. We show the calculated x-ray absorption spectrum for carbon monoxide in Fig. 1 in the energy range of the O $1s \rightarrow \pi^*$ resonance. The PESs were calculated using the quadruple-zeta Dunning basis cc-pVQZ [54] at the level of MRCI by using the quantum chemistry code COLUMBUS [55]. In the equilibrium distance the molecule is well described by a single reference, and it is a good approximation to calculate the electric dipole and Auger transitions at the single reference level (see, for example, Ref. [56]). We consider a spatial grid for the internuclear distance from 1.2 to 25 a.u., with a spatial resolution of $dR = 0.01$ a.u. We solve the TDSE-IS using a fourth-order Runge-Kutta method. We observe that the vibrational structure of the resonance is perfectly resolved in spite of the spatial coordinate representation of the TDSE-IS. The energy spacing matches very well with the experiment; this is mainly due to the good description of the PES for the core-hole state. In the calculations we approximate the electric dipole moment calculated at the equilibrium distance to be equal at all nuclear geometries. As the initial wave packet in the ground state is well localized, this approximation is quite good and results in a good agreement between the relative peaks of the vibrational states in the spectrum. Note that no detector or natural width broadening has been used in the calculated spectrum; the represented black line is directly obtained from the TDSE-IS calculations.

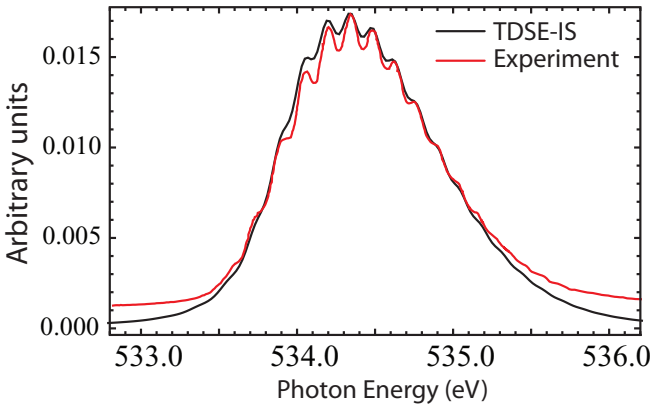

FIG. 1. X-ray absorption spectrum for CO in the energy range of the O $1s \rightarrow \pi^*$ resonance. The TDSE-IS was solved for 50-fs x-ray pulses at different photon energies with 10^{13} W/cm^2 peak intensity. The vibrational states of the electronic $1s^{-1}\pi^*$ level is resolved. The experimental data are taken from Ref. [53].

Similarly, for time-resolved studies we can keep track of the population in the transient states induced by the pump pulse and then obtain the transient x-ray absorption spectrum by taking the population difference before and after the probe pulse.

B. Auger electron spectroscopy

Auger electron spectroscopy is a common technique used in gas-phase experiments and surfaces of condensed-matter systems [57]. This technique is based on detecting the Auger electron emitted after core-hole decay. Because we may select a particular electronic state by detecting the Auger electron, we can retrieve information about the electronic configuration of the system. Also, the Auger electron may be emitted from the valence shell and thus provides information about the local chemical environment with respect to the absorber.

The calculation of the Auger electron spectrum using the TDSE-IS will be slightly different for the resonant and nonresonant core excitations. We start by discussing the nonresonant case, in which two electrons are located in the continuum: the photoelectron and the Auger electron. Within the TDSE-IS framework we can calculate the two-electron coincidence measurements, i.e., the measurement of the photoelectron and Auger electron in coincidence, given by

$$P(\varepsilon,\varepsilon_a) = \lim_{t\to\infty} \sum_{ij} \int d\mathbf{R} \left| b_{\varepsilon\varepsilon_a;ij}(\mathbf{R},t) \right|^2. \tag{18}$$

In the formula above, although it is not written explicitly, we also consider the sum over the other quantum numbers of the photoelectron and Auger electron. If we are also interested in the angular resolution of the emitted electrons, then we need to remove the sum over the orbital angular momenta of the continuum orbitals. The photoelectron spectrum and the

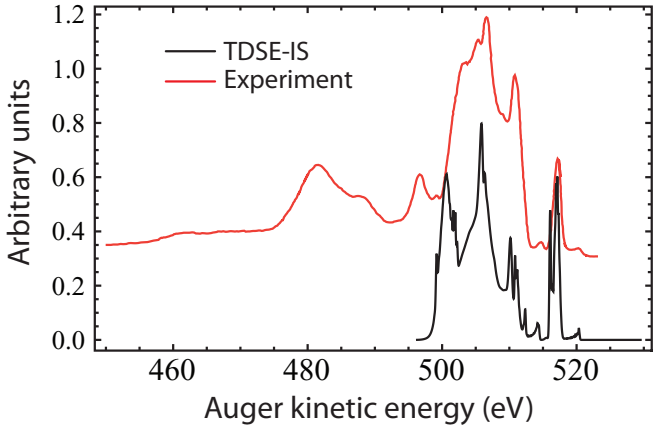

FIG. 2. Auger electron spectrum for CO excited at 534.5 eV in the O $1s \rightarrow \pi^*$ resonance. The TDSE-IS was solved for a 50-fs x-ray pulse with 10^{13} W/cm^2 peak intensity. The experimental data are taken from Ref. [56].

Auger spectrum are then given by

$$P_{ph}(\varepsilon) = \sum_{\varepsilon_a} P(\varepsilon,\varepsilon_a), \tag{19}$$

$$P_a(\varepsilon_a) = \sum_{\varepsilon} P(\varepsilon,\varepsilon_a), \tag{20}$$

respectively. In the resonant case, the previous formulas of the Auger electron spectrum are reduced to

$$P_a(\varepsilon_a) = \lim_{t\to\infty} \sum_{ij} \int d\mathbf{R} \left| b_{c\varepsilon_a;ij}(\mathbf{R},t) \right|^2. \tag{21}$$

In Fig. 2 we show the Auger decay spectrum for CO at 534.5 eV in the O $1s \rightarrow \pi^*$ resonance. In the TDSE-IS, we have included only the 13 dominant low-lying excited states after Auger decay, corresponding to the emission of Auger electrons with high kinetic energies. The calculated Auger spectrum is in good agreement with the experimental spectrum of Ref. [56]. In the calculated spectrum we are able to observe vibrational structures, while they are smoothed out in the experimental spectrum. This could be due to the 350 meV electron energy resolution of the experiment. Also, the peaks located in the calculated spectrum around 500 eV should be shifted to higher kinetic energy by 3 eV. However, the spectrum is overall well described, and this clearly shows the versatility of the TDSE-IS to obtain observables that can be measured in experiments.

V. CONCLUSIONS

In conclusion, we have derived a theoretical approach that accounts for both x-ray excitation and electron relaxation of the core hole in a time-dependent framework. This approach allows us to describe and explore the underlying mechanism of few-femtosecond and attosecond x-ray pulses interacting with molecules. This might open the possibility to explore the role of Auger processes in the coherent evolution of the nuclear wave packets as well as nonadiabatic effects during x-ray excitation. Also, the introduced theoretical approach is ideal for calculating momentum distribution retrieved from electron-ion coincidence measurements, which are very sensitive to both electronic configurations and nuclear geometries. These techniques will be significantly enhanced at future x-ray sources with high-repetition-rate capabilities. The introduced framework can also be extended in order to include the interaction of a strong-field laser with the system and thus to study interesting topics of charge migration in molecules with high-harmonic generation [58–60]. The strong-field laser is well described within the strong-field approximation (SFA), and the connection between the SFA and a quantum formalism has been shown in Ref. [61], which can be adapted to the present framework. This will enable us to explore the SFA in molecules in both the ionization and the Auger-decay steps [62,63]. Within this formalism we could also explore electron dynamics induced by the coupling between different core-hole states, analogous to previous approaches used in atomic systems [64,65].

ACKNOWLEDGMENTS

A.P. is grateful to C. Bostedt for inspiring this project, scientific discussions, and his support. This material is based upon work supported by the U.S. Department of Energy, Office of Science, Basic Energy Sciences, Chemical Sciences, Geosciences, and Biosciences Division and supported by the Argonne group under Contract No. DE-AC02-06CH11357. A.P. also acknowledges support from the European Union's Horizon 2020 research and innovation program under Marie Sklodowska-Curie Grant Agreement No. 702565.

APPENDIX: ADIABATIC APPROXIMATION

In this appendix we derive the adiabatic approximation of the Auger transition step. We start by taking the integral form of Eq. (13),

$$b_{\varepsilon\varepsilon_a;ij}(\mathbf{R},t) = -i e^{-i[\hat{H}_n + E_{\varepsilon\varepsilon_a;ij}(\mathbf{R})]t} \int_0^t dt' e^{i[\hat{H}_n + E_{\varepsilon\varepsilon_a;ij}(\mathbf{R})]t'} \times \sum_{\varepsilon' i'} \langle \varepsilon\varepsilon_a; ij | V_r | \varepsilon'; i' \rangle \, b_{\varepsilon';i'}(\mathbf{R},t),$$

and including this form in Eq. (12) to obtain a new equation without the amplitudes of the final states,

$$\begin{aligned} i\,\dot{b}_{\varepsilon;i}(\mathbf{R},t) = {} & [\hat{H}_n + E_{\varepsilon;i}(\mathbf{R})] b_{\varepsilon;i}(\mathbf{R},t) + \langle \varepsilon; i | V_I(t) | 0 \rangle \, b_0(\mathbf{R},t) \\ & - i \sum_{\varepsilon'' \varepsilon_a''} \sum_{i'' j''} \langle \varepsilon; i | V_r | \varepsilon'' \varepsilon_a''; i'' j'' \rangle \, e^{-i[\hat{H}_n + E_{\varepsilon'' \varepsilon_a'';i'' j''}(\mathbf{R})]t} \\ & \times \int_0^t dt' e^{i[\hat{H}_n + E_{\varepsilon'' \varepsilon_a'';i'' j''}(\mathbf{R})]t'} \\ & \times \sum_{\varepsilon' i'} \langle \varepsilon'' \varepsilon_a''; i'' j'' | V_r | \varepsilon'; i' \rangle \, b_{\varepsilon';i'}(\mathbf{R},t'). \end{aligned}$$

The second line can be reduced to a decay rate Γ factor that accounts for the Auger decay yield and a Stark shift R factor that accounts for the dephasing. In order to perform the integration in the second line, the core-hole amplitude $b_{\varepsilon';i'}(\mathbf{R},t')$ needs to be expressed in the eigenbasis of the operator $[\hat{H}_n + E_{\varepsilon'' \varepsilon_a'';i'' j''}(\mathbf{R})]$. Therefore, we express the

core-hole amplitude as

$$b_{\varepsilon';i'}(\mathbf{R},t') = \sum_{\nu} c_{\nu,\varepsilon' i'}(t')\, b_{\nu,\varepsilon' i'}(\mathbf{R}) = \sum_{\nu\nu'} c_{\nu,\varepsilon' i'}(t')\, t_{\nu,\varepsilon' i'}^{\nu',\varepsilon'' \varepsilon_a'' i'' j''}\; b_{\nu',\varepsilon'' \varepsilon_a'' i'' j''}(\mathbf{R}),$$

where first we expand the core-hole state nuclear wave packet in the core-hole vibrational basis, then every vibrational core-hole state wave function is expanded in vibrational states of the electronic level $\varepsilon'' \varepsilon_a'' i'' j''$, with $t_{\nu,\varepsilon' i'}^{\nu',\varepsilon'' \varepsilon_a'' i'' j''}$ being the coefficients of the transformation (related to the Frank-Condon factors). Now we use this expansion in order to convert the operators $[\hat{H}_n + E_{\varepsilon'' \varepsilon_a'';i'' j''}(\mathbf{R})]$ into energies to be able to perform the integration over time t':

$$\begin{aligned} i\,\dot{b}_{\varepsilon;i}(\mathbf{R},t) = {} & [\hat{H}_n + E_{\varepsilon;i}(\mathbf{R})] b_{\varepsilon;i}(\mathbf{R},t) + \langle \varepsilon; i | V_I(t) | 0 \rangle\, b_0(\mathbf{R},t) \\ & - i \sum_{\varepsilon'' \varepsilon_a''} \sum_{i'' j''} \sum_{\nu\nu'} \langle \varepsilon; i | V_r | \varepsilon'' \varepsilon_a''; i'' j'' \rangle\, e^{-i E_{\nu',\varepsilon'' \varepsilon_a'' i'' j''} t} \int_0^t dt' t_{\nu,\varepsilon' i'}^{\nu',\varepsilon'' \varepsilon_a'' i'' j''} e^{i E_{\nu',\varepsilon'' \varepsilon_a'' i'' j''} t'} \\ & \times \sum_{\varepsilon' i'} \langle \varepsilon'' \varepsilon_a''; i'' j'' | V_r | \varepsilon'; i' \rangle\, c_{\nu,\varepsilon' i'}(t')\, b_{\nu',\varepsilon'' \varepsilon_a'' i'' j''}(\mathbf{R}), \end{aligned}$$

assuming that $\langle \varepsilon'' \varepsilon_a''; i'' j'' | V_r | \varepsilon'; i' \rangle$ slowly changes with $\mathbf{R}$. Within the adiabatic (Markov) approximation, we split the time-dependent factors into slow and fast time variants:

$$c_{\nu,\varepsilon' i'}(t') = \tilde{c}_{\nu,\varepsilon' i'}(t') e^{-i E_{\nu,\varepsilon' i'} t'},$$

and we will have a new integral that can be written as

$$\int_{t_0}^{t} dt' e^{i E_{\nu',\varepsilon'' \varepsilon_a'' i'' j''} t'} e^{-i E_{\nu,\varepsilon' i'} t'} \approx \pi\, \delta\left(E_{\nu',\varepsilon'' \varepsilon_a'' i'' j''} - E_{\nu,\varepsilon' i'}\right) e^{i(E_{\nu',\varepsilon'' \varepsilon_a'' i'' j''} - E_{\nu,\varepsilon' i'}) t} - i\, P\left[\frac{1}{E_{\nu',\varepsilon'' \varepsilon_a'' i'' j''} - E_{\nu,\varepsilon' i'}}\right] e^{i(E_{\nu',\varepsilon'' \varepsilon_a'' i'' j''} - E_{\nu,\varepsilon' i'}) t},$$

where P stands for the principal part. Hence, the integration is split into two terms, and the previous EOM is then reduced to

$$\begin{aligned} i\,\dot{b}_{\varepsilon;i}(\mathbf{R},t) = {} & [\hat{H}_n + E_{\varepsilon;i}(\mathbf{R})] b_{\varepsilon;i}(\mathbf{R},t) + \langle \varepsilon; i | V_I(t) | 0 \rangle\, b_0(\mathbf{R},t) \\ & - i \sum_{\varepsilon' i'} \sum_{\varepsilon'' \varepsilon_a''} \sum_{i'' j''} \sum_{\nu\nu'} \pi\, \delta\left(E_{\nu',\varepsilon'' \varepsilon_a'' i'' j''} - E_{\nu,\varepsilon' i'}\right) \langle \varepsilon; i | V_r | \varepsilon'' \varepsilon_a''; i'' j'' \rangle\, \langle \varepsilon'' \varepsilon_a''; i'' j'' | V_r | \varepsilon'; i' \rangle c_{\nu,\varepsilon' i'}(t)\, t_{\nu,\varepsilon' i'}^{\nu',\varepsilon'' \varepsilon_a'' i'' j''}\; b_{\nu',\varepsilon'' \varepsilon_a'' i'' j''}(\mathbf{R}) \\ & - \sum_{\varepsilon' i'} \sum_{\varepsilon'' \varepsilon_a''} \sum_{i'' j''} \sum_{\nu\nu'} P\left[\frac{1}{E_{\nu',\varepsilon'' \varepsilon_a'' i'' j''} - E_{\nu,\varepsilon' i'}}\right] \langle \varepsilon; i | V_r | \varepsilon'' \varepsilon_a''; i'' j'' \rangle\, \langle \varepsilon'' \varepsilon_a''; i'' j'' | V_r | \varepsilon'; i' \rangle c_{\nu,\varepsilon' i'}(t)\, t_{\nu,\varepsilon' i'}^{\nu',\varepsilon'' \varepsilon_a'' i'' j''}\; b_{\nu',\varepsilon'' \varepsilon_a'' i'' j''}(\mathbf{R}). \end{aligned}$$

Note in the second line that from the sum over all the vibrational states in the core-hole state ν and the final dication state ν', the energy conservation imposed by the δ function fixed the value of the Auger electron energy. Therefore, for every (ν,ν') we have a different Auger electron energy determined by the energy conservation. If we assume that the Auger matrix transitions $\langle \varepsilon'' \varepsilon_a''; i'' j'' | V_r | \varepsilon'; i' \rangle$ slowly change with the Auger energy electron ε_a and the Frank-Condon-factor-related products $t_{\nu,\varepsilon' i'}^{\nu',\varepsilon'' \varepsilon_a'' i'' j''}\; b_{\nu',\varepsilon'' \varepsilon_a'' i'' j''}(\mathbf{R})$ also slowly change on ε_a (as is expected because they should be mainly dependent on the PES of the electronic core-hole and dication levels), we can finally derive the second equation of the EOMs (14) by defining

$$\frac{\Gamma_{\varepsilon i,\varepsilon' i'}(\mathbf{R})}{2} = \pi \sum_{\varepsilon'' \varepsilon_a'} \sum_{i'' j''} \langle \varepsilon; i | V_r | \varepsilon'' \varepsilon_a''; i'' j'' \rangle\, \langle \varepsilon'' \varepsilon_a''; i'' j'' | V_r | \varepsilon'; i' \rangle\;\; \delta\left(E_{\varepsilon'' \varepsilon_a'';i'' j''} - E_{\varepsilon';i'}\right),$$

$$R_{\varepsilon i,\varepsilon' i'}(\mathbf{R}) = -i \sum_{i'' j''} \langle \varepsilon; i | V_r | \varepsilon'' \varepsilon_a''; i'' j'' \rangle\, \langle \varepsilon'' \varepsilon_a''; i'' j'' | V_r | \varepsilon'; i' \rangle\;\; P\left[\frac{1}{E_{\varepsilon'' \varepsilon_a'';i'' j''} - E_{\varepsilon';i'}}\right].$$

Similarly, we can use the adiabatic approximation in the ionization step in order to derive the first equation of the EOMs (14). First, we take the integral form of the second equation (14), and we substitute it into Eq. (11). We obtain an integral over t'. Following a procedure similar to that in the previous calculations, we divide the time-dependent factors into slow and fast time variants. Then we perform the integration, and we obtain an ionization rate Γ_I and a Stark shift R_I factor.

[1] K. Siegbahn, Electron spectroscopy for atoms, molecules, and condensed matter, Science **217**, 111 (1982).

[2] *Theory of Photoionization: VUV and Soft X-ray Frequency Region*, edited by U. Becker and D. A. Shirley (Plenum, New York, 1996).

[3] J. Stöhr, *NEXAFS Spectroscopy*, Springer Series in Surface Sciences Vol. 25 (Springer, Berlin, 2010).

[4] A. H. Zewail, Femtochemistry: Atomic-scale dynamics of the chemical bond, J. Phys. Chem. A **104**, 5660 (2000).

[5] O. Gessner and M. Gühr, Monitoring ultrafast chemical dynamics by time-domain X-ray photo- and auger-electron spectroscopy, Acc. Chem. Res. **49**, 138 (2015).

[6] M. Chergui, Time-resolved X-ray spectroscopies of chemical systems: New perspectives, Struct. Dyn. **3**, 031001 (2016).

[7] C. Bostedt *et al.*, Linac coherent light source: The first five years, Rev. Mod. Phys. **88**, 015007 (2016).

[8] F. Bencivenga, F. Capotondi, E. Principi, M. Kiskinova, and C. Masciovecchio, Coherent and transient states studied with extreme ultraviolet and X-ray free electron lasers: Present and future prospects, Adv. Phys. **63**, 327 (2015).

[9] J. Feldhaus, M. Krikunova, M. Meyer, Th. Möller, R. Moshammer, A. Rudenko, Th. Tschentscher, and J. Ullrich, AMO science at the FLASH and European XFEL free-electron laser facilities, J. Phys. B **46**, 164002 (2013).

[10] M. Yabashi *et al.*, Compact XFEL and AMO sciences: SACLA and SCSS, J. Phys. B **46**, 164001 (2013).

[11] M.-C. Chen *et al.*, Generation of bright isolated attosecond soft X-ray pulses driven by multicycle midinfrared lasers, Proc. Natl. Acad. Sci. U.S.A. **111**, E2361 (2014).

[12] D. Fabris *et al.*, Synchronized pulses generated at 20 eV and 90 eV for attosecond pump-probe experiments, Nat. Photonics **9**, 383 (2015).

[13] S. L. Cousin, F. Silva, S. Teichmann, M. Hemmer, B. Buades, and J. Biegert, High-flux table-top soft x-ray source driven by sub-2-cycle, CEP stable, 1.85-mu m 1-kHz pulses for carbon K-edge spectroscopy, Opt. Lett. **39**, 5383 (2014).

[14] F. Silva, S. M. Teichmann, S. L. Cousin, and J. Biegert, Spatiotemporal isolation of attosecond soft X-ray pulses in the water window, Nat. Commun. **6**, 6611 (2015).

[15] C. Hernández-García, T. Popmintchev, M. M. Murnane, H. C. Kapteyn, L. Plaja, A. Becker, and A. Jaron-Becker, Group velocity matching in high-order harmonic generation driven by mid-infrared lasers, New J. Phys. **18**, 073031 (2016).

[16] K. Ramasesha, S. R. Leone, and D. M. Neumark, Real-time probing of electron dynamics using attosecond time-resolved spectroscopy, Annu. Rev. Phys. Chem. **67**, 41 (2016).

[17] A. Rudenko *et al.*, Exploring few-photon, few-electron reactions at FLASH: From ion yield and momentum measurements to time-resolved and kinematically complete experiments, J. Phys. B **43**, 194004 (2010).

[18] M. Magrakvelidze *et al.*, Tracing nuclear-wave-packet dynamics in singly and doubly charged states of N_2 and O_2 with XUV-pump–XUV-probe experiments, Phys. Rev. A **86**, 013415 (2012).

[19] C. E. Liekhus-Schmaltz *et al.*, Ultrafast isomerization initiated by x-ray core ionization, Nat. Commun. **6**, 8199 (2015).

[20] K. R. Ferguson, M. Bucher, T. Gorkhover, S. Boutet, H. Fukuzawa, J. E. Koglin, Y. Kumagai, A. Lutman, A. Marinelli, M. Messerschmidt, K. Nagaya, J. Turner, K. Ueda, G. J. Williams, P. H. Bucksbaum, and C. Bostedt, Transient lattice contraction in the solid-to-plasma transition, Sci. Adv. **2**, e1500837 (2016).

[21] A. Picón *et al.*, Hetero-site-specific X-ray pump-probe spectroscopy for femtosecond intramolecular dynamics, Nat. Commun. **7**, 11652 (2016).

[22] C. S. Lehmann *et al.*, Ultrafast x-ray-induced nuclear dynamics in diatomic molecules using femtosecond x-ray-pump–x-ray-probe spectroscopy, Phys. Rev. A **94**, 013426 (2016).

[23] S. Mukamel *et al.*, Coherent multidimensional optical probes for electron correlations and exciton dynamics: From NMR to X-rays, Acc. Chem. Res. **42**, 553 (2009).

[24] E. Pahl, H.-D. Meyer, and L. S. Cederbaum, Competition between excitation and electronic decay of short-lived molecular states, Z. Phys. D **38**, 215 (1996).

[25] P. V. Demekhin, Y.-C. Chiang, and L. S. Cederbaum, Resonant Auger decay of the core-excited C^*O molecule in intense x-ray laser fields, Phys. Rev. A **84**, 033417 (2011).

[26] S. Yabushita, C. W. McCurdy, and T. N. Rescigno, Complex-basis-function treatment of photoionization in the random-phase approximation, Phys. Rev. A **36**, 3146 (1987).

[27] R. R. Lucchese and R. W. Zurales, Comparison of the random-phase approximation with the multichannel frozen-core Hartree-Fock approximation for the photoionization of N_2, Phys. Rev. A **44**, 291 (1991).

[28] P. Lin and R. R. Lucchese, Theoretical studies of core excitation and ionization in molecular systems, J. Synchrotron Radiat. **8**, 150 (2001).

[29] N. A. Cherepkov and S. K. Semenov, New developments in the theory of molecular K-shell photoionization, Int. J. Quantum Chem. **107**, 2889 (2007).

[30] J. Schirmer and F. Mertins, A new approach to the random phase approximation, J. Phys. B **29**, 3559 (1996).

[31] T. Aberg and G. Howat, Theory of the auger effect, in *Encyclopedia of Physics: Corpuscles and Radiation in Matter I*, edited by S. Flügge and W. Mehlhorn, Handbuch der Physik Vol. 31 (Springer, Berlin, 1982), p. 469.

[32] L. S. Cederbaum and W. Domcke, Local against non-local complex potential in resonant electron-molecule scattering, J. Phys. B **14**, 4665 (1981).

[33] W. Domcke, Theory of resonance and threshold effects in electron-molecule collisions: The projection-operator approach, Phys. Rep. **208**, 97 (1991).

[34] *Frontiers of Laser Spectroscopy*, edited by C. Cohen-Tannoudji, R. Balian, S. Haroche, and S. Liberman (North-Holland, Amsterdam, 1977).

[35] P. L. Knight, M. A. Lauder, and B. J. Dalton, Laser-induced continuum structure, Phys. Rep. **190**, 1 (1990).

[36] H. Agren, V. Carravetta, O. Vahtras, and L. G. M. Pettersson, Direct, atomic orbital, static exchange calculations of photoabsorption spectra of large molecules and clusters, Chem. Phys. Lett. **222**, 75 (1994).

[37] S. Shirai, S. Yamamoto, and S.-A. Hyodo, Accurate calculation of core-electron binding energies: Multireference perturbation treatment, J. Chem. Phys. **121**, 7586 (2004).

[38] N. A. Besley, A. T. B. Gilbert, and P. M. W. Gill, Self-consistent-field calculations of core excited states, J. Chem. Phys. **130**, 124308 (2009).

[39] J. V. Ortiz, Toward an exact one-electron picture of chemical bonding, Adv. Quantum Chem. **35**, 33 (1999).

[40] S. Gozem, A. O. Gunina, T. Ichino, D. L. Osborn, J. F. Stanton, and A. I. Krylov, Photoelectron wave function in photoionization: Plane wave or coulomb wave?, J. Phys. Chem. Lett. **6**, 4532 (2015).

[41] R. R. Lucchese, G. Raseev, and V. McKoy, Studies of differential and total photoionization cross sections of molecular nitrogen, Phys. Rev. A **25**, 2572 (1982).

[42] P. V. Demekhin, A. Ehresmann, and V. L. Sukhorukov, Single center method: A computational tool for ionization and electronic excitation studies of molecules, J. Chem. Phys. **134**, 024113 (2011).

[43] P. B. Burke, *R-Matrix Theory of Atomic Collisions: Application to Atomic, Molecular and Optical Processes*, Springer Series on Atomic, Optical, and Plasma Physics Vol. 61 (Springer, Berlin, 2011).

[44] M. Tarana and J. Horáček, Correlation effects in R-matrix calculations of electron-F_2 elastic scattering cross sections, J. Chem. Phys. **127**, 154319 (2007).

[45] P. W. Langhoff, Stieltjes imaging of atomic and molecular photoabsorption profiles, Chem. Phys. Lett. **22**, 60 (1973).

[46] J. Cukras, S. Coriani, P. Decleva, O. Christiansen, and P. Norman, Photoionization cross section by Stieltjes imaging applied to coupled cluster Lanczos pseudo-spectra, J. Chem. Phys. **139**, 094103 (2013).

[47] V. Averbukh and L. S. Cederbaum, *Ab initio* calculation of interatomic decay rates by a combination of the Fano ansatz, Green's-function methods, and the Stieltjes imaging technique, J. Chem. Phys. **123**, 204107 (2005).

[48] D. Moonshiram *et al.*, Tracking the structural and electronic configurations of a cobalt proton reduction catalyst in water, J. Am. Chem. Soc. **138**, 10586 (2016).

[49] D. Moonshiram *et al.*, Mechanistic evaluation of a nickel proton reduction catalyst using time-resolved X-ray absorption spectroscopy, J. Phys. Chem. C **120**, 20049 (2016).

[50] C. Bressler and M. Chergui, Molecular structural dynamics probed by ultrafast X-ray absorption spectroscopy, Annu. Rev. Phys. Chem. **61**, 263 (2010).

[51] J. Yano and V. K. Yachandra, X-ray absorption spectroscopy, Photosynth. Res. **102**, 241 (2009).

[52] X. Zhang *et al.*, Visualizing interfacial charge transfer in Ru-dye-sensitized TiO_2 nanoparticles using X-ray transient absorption spectroscopy, J. Phys. Chem. Lett. **2**, 628 (2011).

[53] R. Püttner *et al.*, Vibrationally resolved O 1*s* core-excitation spectra of CO and NO, Phys. Rev. A **59**, 3415 (1999).

[54] T. H. Dunning, Gaussian basis sets for use in correlated molecular calculations. I. The atoms boron through neon and hydrogen, J. Chem. Phys. **90**, 1007 (1989).

[55] H. Lischka, R. Shepard, R. M. Pitzer, I. Shavitt, M. Dallos, Th. Müller, P. G. Szalay, M. Seth, G. S. Kedziora, S. Yabushita and Z. Zhang, High-level multireference methods in the quantum-chemistry program system COLUMBUS: Analytic MR-CISD and MR-AQCC gradients and MR-AQCC-LRT for excited states, GUGA spinorbit CI and parallel CI density, Phys. Chem. Chem. Phys. **3**, 664 (2001).

[56] M. N. Piancastelli, M. Neeb, A. Kivimäki, B. Kempgens, H. M. Köppe, K. Maier, A. M. Bradshaw, and R. F. Fink, Vibrationally resolved 1s $\rightarrow 2\pi$ decay spectra of CO at the C and O K-edges: Experiment and theory, J. Phys. B **30**, 5677 (1997).

[57] D. Briggs and J. T. Grant, *Surface Analysis by Auger and X-ray Photoelectron Spectroscopy* (IM Publications, Chichester, UK, 2003).

[58] F. Lépine, M. Y. Ivanov, and M. J. J. Vrakking, Attosecond molecular dynamics: Fact or fiction?, Nat. Photonics **8**, 195 (2014).

[59] S. R. Leone and D. M. Neumark, Attosecond science in atomic, molecular, and condensed matter physics, Faraday Discuss. **194**, 15 (2016).

[60] P. M. Kraus, B. Mignolet, D. Baykusheva, A. Rupenyan, L. Horný, E. F. Penka, G. Grassi, O. I. Tolstikhin, J. Schneider, F. Jensen, L. B. Madsen, A. D. Bandrauk, F. Remacle, H. J. Wörner, Measurement and laser control of attosecond charge migration in ionized iodoacetylene, Science **350**, 790 (2015).

[61] M. Lewenstein, Ph. Balcou, M. Yu. Ivanov, A. L'Huillier, and P. B. Corkum, Theory of high-harmonic generation by low-frequency laser fields, Phys. Rev. A **49**, 2117 (1994).

[62] A. Picón, C. Buth, G. Doumy, B. Krässig, L. Young, and S. H. Southworth, Optical control of resonant Auger processes, Phys. Rev. A **87**, 013432 (2013).

[63] A. Picón, P. J. Ho, G. Doumy and S. H Southworth, Optically-dressed resonant Auger processes induced by high-intensity x-rays, New J. Phys. **15**, 083057 (2013).

[64] S. Pabst, L. Greenman, P. J. Ho, D. A. Mazziotti, and R. Santra, Decoherence in Attosecond Photoionization, Phys. Rev. Lett. **106**, 053003 (2011).

[65] S. Pabst and R. Santra, Strong-Field Many-Body Physics and the Giant Enhancement in the High-Harmonic Spectrum of Xenon, Phys. Rev. Lett. **111**, 233005 (2013).